Thermoelectric Materials

International Edition: DOI: 10.1002/anie.201605015
German Edition: DOI: 10.1002/ange.201605015

Concerted Rattling in $CsAg_5Te_3$ Leading to Ultralow Thermal Conductivity and High Thermoelectric Performance

Hua Lin[+], Gangjian Tan[+], Jin-Ni Shen, Shiqiang Hao, Li-Ming Wu, Nicholas Calta, Christos Malliakas, Si Wang, Ctirad Uher, Christopher Wolverton, and Mercouri G. Kanatzidis**

Abstract: *Thermoelectric (TE) materials convert heat energy directly into electricity, and introducing new materials with high conversion efficiency is a great challenge because of the rare combination of interdependent electrical and thermal transport properties required to be present in a single material. The TE efficiency is defined by the figure of merit $ZT = (S^2\sigma)T/\kappa$, where S is the Seebeck coefficient, σ is the electrical conductivity, κ is the total thermal conductivity, and T is the absolute temperature. A new p-type thermoelectric material, $CsAg_5Te_3$, is presented that exhibits ultralow lattice thermal conductivity (ca. 0.18 $Wm^{-1}K^{-1}$) and a high figure of merit of about 1.5 at 727 K. The lattice thermal conductivity is the lowest among state-of-the-art thermoelectrics; it is attributed to a previously unrecognized phonon scattering mechanism that involves the concerted rattling of a group of Ag ions that strongly raises the Grüneisen parameters of the material.*

Thermoelectrics (TE) are important functional materials that are able to directly convert thermal energy to electricity and can enable power generation from many heat sources including waste heat.[1,2] The efficiency of thermoelectrics (ZT) can be enhanced by various strategies of increasing the power factor ($PF = S^2\sigma$) and/or reducing the thermal conductivity, such as band engineering,[3] resonant states,[4] energy barrier filtering,[5] and all-scale nanostructuring.[6] Another strategy is to explore materials possessing intrinsically low thermal conductivities.[7–11] Recent studies reveal that highly disordered or layered compounds exhibit low thermal conductivities and high ZT values, such as $Cu_{2-x}S$, $Cu_{2-x}Se$, $AgSbSe_2$, and tetrahedrites, with thermal conductivities ranging from 0.35 and 0.60 $W m^{-1} K^{-1}$.[12–15] Two examples that do not exhibit structural disorder but still possess very low thermal conductivities are the highly anisotropic In_4Se_3[9] and SnSe.[16,17] The former shows ZT values of 1.4 along the *bc* plane with very low thermal conductivity (0.70 $W m^{-1} K^{-1}$) at 700 K,[9] and the latter ZT values of 2.6, or 2.3 along the *b* or *c* axis, respectively, at 973 K with ultra-low thermal conductivity (ca. 0.45 $W m^{-1} K^{-1}$ at 973 K).[16,17] Therefore, materials with intrinsically very low thermal conductivity are highly desirable in the search for high TE performance. Herein we present $CsAg_5Te_3$, a new exceptional TE material with an even lower thermal conductivity than SnSe. This thermal behavior is achieved by a new phonon scattering mechanism that we call concerted rattling, which enables $CsAg_5Te_3$ to reach a ZT of 1.5 at 727 K without any extrinsic doping.

The synthesis and single crystal structure of $CsAg_5Te_3$ was first reported in 1995 by Li et al.[18] In this work, we study the thermoelectric properties of this compound and, surprisingly, find that $CsAg_5Te_3$ exhibits intrinsically ultralow lattice thermal conductivity (0.18–0.14 $W m^{-1} K^{-1}$). We explain this on the basis of the special phonon band structure that involves peculiar low frequency rattling modes in the Ag sublattice. These Ag atoms give rise to very large Grüneisen parameters, and hence, anharmonic vibrations. As a result, $CsAg_5Te_3$ exhibits a figure of merit of about 1.5 at 727 K (Figure 1 A), among the highest for any single-phase compound, distinguishing itself as a new promising mid-temperature TE material.

Pure polycrystalline $CsAg_5Te_3$ samples were prepared by melting Ag, Te elements and Cs_2Te_3 with stoichiometric ratio in a fused silica tube at 1073 K for 2 h and then cooled to room temperature. The ingot was ground into fine powders, and then densified by spark plasma sintering method (SPS-211LX, Fuji Electronic Industrial Co. Ltd.) at 723 K under a pressure of 50 MPa for 10 min. The obtained pellets had mass densities of $>97\%$ of the theoretical value (7.117 $g cm^{-3}$) and were cut with a diamond blade saw to suitable sized specimens for measurements (Figure 1 A, inset).

Because of the remarkably low lattice thermal conductivity, we wanted to take a more detailed look at its crystal structure and particularly the atomic displacement parameters (ADPs), seeking useful insights. We collected accurate single crystal X-ray diffraction data for $CsAg_5Te_3$ at room

[*] Dr. H. Lin,[+] Dr. J. N. Shen, Prof. L. M. Wu
Key Laboratory of Design and Assembly of Functional Nanostructures, Fujian Institute of Research on the Structure of Matter
Chinese Academy of Sciences
Fuzhou, Fujian 350002 (P.R. China)
E-mail: liming_wu@fjirsm.ac.cn
Dr. G. Tan,[+] Dr. N. Calta, Dr. C. Malliakas, Prof. M. G. Kanatzidis
Department of Chemistry, Northwestern University
Evanston, IL 60208 (USA)
E-mail: m-kanatzidis@northwestern.edu
Dr. S. Q. Hao, Dr. N. Calta, Prof. C. Wolverton
Department of Materials Science and Engineering
Northwestern University, Evanston, IL 60208 (USA)
S. Wang
State Key Laboratory of Advanced Technology for Materials Synthesis and Processing, Wuhan University of Technology
Wuhan 430070 (China)
S. Wang, Prof. C. Uher
Department of Physics, University of Michigan
Ann Arbor, MI 48109 (USA)
[+] These authors contributed equally to this work.
Supporting information and the ORCID identification number(s) for the author(s) of this article can be found under: http://dx.doi.org/10.1002/anie.201605015.

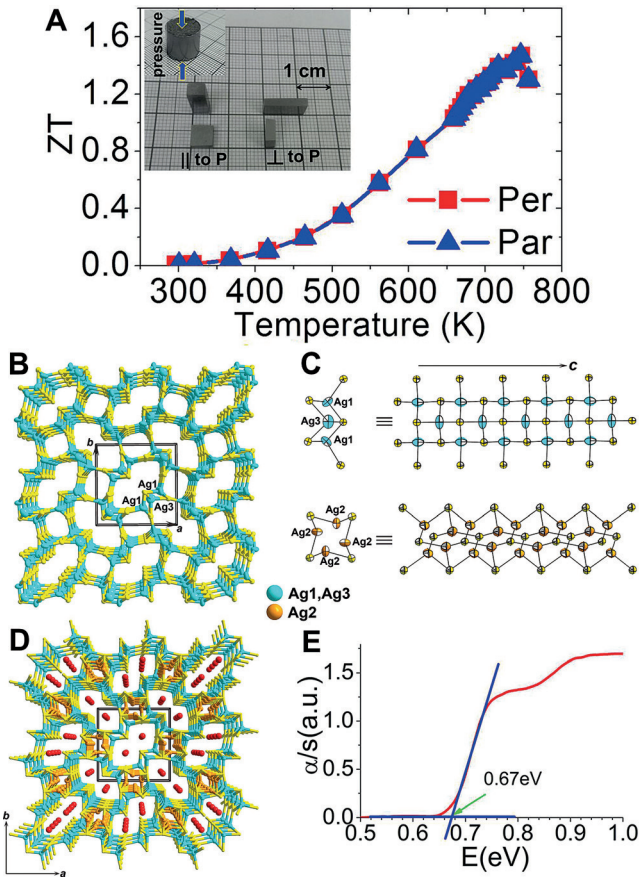

Figure 1. *ZT* values, crystal structure, and band gap of $CsAg_5Te_3$. A) The temperature dependence of *ZT* temperature. Inset: photos of sample and the cut specimens (cut along the perpendicular direction of SPS pressure and parallel to the direction of SPS pressure). B) Perspective view of the open tunnel network constructed by strong covalent bonding interactions of the three $AgTe_4$-wide-chains (defined by Ag1 and Ag3) creating large-, and small-size-tunnels locating at the center/origin, and the side of the unit cell, respectively. Yellow atoms: Te. C) A single chain constructed by Ag1, Ag3 atoms that adopt common tetrahedral coordination (top) and a single $[AgTe^-]_n$ column constructed by weakly bonded Ag2 atoms that are coordinated in triangular planar geometry (bottom). Ellipsoids are set at 95% probability. D) Overall crystal structure of $CsAg_5Te_3$, in which Cs atoms (red) and weakly bonded Ag2 atoms are accommodated in the large-, and small-size-tunnel, respectively. E) Electronic absorption spectrum and energy band gap of a sample of $CsAg_5Te_3$.

temperature (RT) and at 100 K. No phase transitions were observed in this temperature range. $CsAg_5Te_3$ crystallizes in the tetragonal space group $P4_2/mnm$ with $a = b = 14.645(2)$ Å, $c = 4.5907(9)$ Å (at RT), and $a = b = 14.567(2)$ Å, $c = 4.5501(9)$ Å (at 100 K; Supporting Information, Table S1). The phase purity for both as-synthesized and spark plasma sintered (SPSed) samples were confirmed by powder X-ray diffraction data (Supporting Information, Figure S1). Several peaks in the difference curve indicate some deviation of the diffraction intensity, which may come from the crystallite orientation preference. According to the subsequent property measurement results, this seems to show no obvious effect on the TE properties. Field emission scanning electron microscopy (FESEM) via back-scattered electron (BSE) imaging shows clean surfaces with no visible pores and the BSE image shows uniformity with no contrast difference, which confirms the pure phases (Supporting Information, Figure S2). The special structural feature of $CsAg_5Te_3$ is the open tunnels, Figure 1B, constructed by infinite parallel $AgTe_4$-chains, Figure 1C. These $AgTe_4$ chains create two types of tunnels within the Ag-Te covalent network that run parallel to the *c* axis: the large-size-tunnels located at the center (0.5, 0.5, 0.5) and the origin (0, 0, 0) of the unit cell, and the small-size tunnels at each side of the unit cell. The Ag1, Ag3 atoms adopt a common tetrahedral coordination with Te atoms and with Ag-Te bonds of 2.743–3.058 Å (Figure 1C, top). In contrast, the Ag2 atoms adopt the less common coplanar triangle coordination geometry with Ag-Te bonds of 2.789–2.886 Å. Such $Ag2Te_3$ triangles form the $[AgTe^-]_n$ column by sharing vertexes (Figure 1C, bottom). Each of the $[AgTe^-]_n$ columns fills in the small-size-tunnel (Figure 1D) while the large tunnels in the structure accommodate the Cs atoms. (Figure 1D). Notably, the Ag atoms have large anisotropic thermal parameters, the largest among all the atoms in the unit cell (Supporting Information, Tables S2, S3), which are implicated in the strong phonon scattering of the material. The optical diffuse reflectance spectroscopy reveals a direct band gap of 0.67 eV (Figure 1E).

$CsAg_5Te_3$ is a semiconductor with electrical conductivity σ gradually increasing from about 0.17 $S\,cm^{-1}$ at RT to about 49 $S\,cm^{-1}$ at 727 K (Figure 2A). Above 730 K, a phase transition occurs and σ drops sharply (Supporting Information, Figure S3). The Hall measurements indicate holes are the dominant charge carriers with a carrier concentration

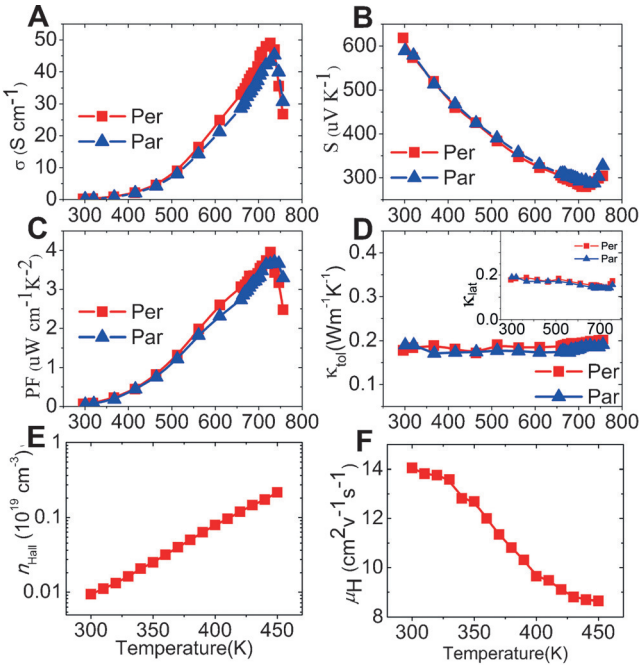

Figure 2. Temperature dependence of thermoelectric properties of the SPSed polycrystalline $CsAg_5Te_3$ (Per: the perpendicular direction of SPS pressure, Par: the parallel direction of SPS pressure). A) Electrical conductivity σ. B) Seebeck coefficient *S*. C) Power factor PF. D) Total thermal conductivity κ_{tot}. Inset: lattice thermal conductivity κ_{lat} of $CsAg_5Te_3$. E) Hall carrier concentration n_{Hall}. F) Hall mobility μ_H.

(n_{Hall}) and Hall mobility (μ_H) of about $1\times10^{17}\,cm^{-3}$ and $14\,cm^2V^{-1}s^{-1}$ at 300 K, respectively (Figure 2 E,F). Such a carrier concentration is 2–3 orders lower than state-of-the-art thermoelectrics (10^{19}–$10^{20}\,cm^{-3}$).[19] The Seebeck coefficients of $CsAg_5Te_3$ are shown as a function of temperature in Figure 2 B. The material exhibits positive Seebeck coefficients from 600 to 300 $\mu V K^{-1}$, in agreement with the p-type behavior of the Hall data.

As shown in Figure 2 C, $CsAg_5Te_3$ exhibits moderate power factors ($PF = S^2\sigma$) with the maximum value of 3.9 $\mu W cm^{-1}K^{-2}$ at 727 K. This value is comparable to those of other thermoelectrics that possess intrinsically low total thermal conductivities (for example, 3.9, 5.7, 6.7, 10.1, 8.2, and 12 $\mu W cm^{-1}K^{-2}$ of Ag_9TlTe_5,[20] $Yb_{14}MnSb_{11}$,[21] Tl_9BiTe_6,[22] b axis of SnSe,[16] α-$Cu_{2-x}S$,[13] and β-$Cu_{2-x}Se$,[12] respectively).

The key and remarkable feature of $CsAg_5Te_3$ is its exceedingly low total thermal conductivity (κ_{tot}), which ranges from 0.18 $W m^{-1}K^{-1}$ at 296 K to 0.20 $W m^{-1}K^{-1}$ at 727 K (Figure 2 D), agreeing well with the values we obtained using a longitudinal steady-state technique at low temperature (Supporting Information, Figure S4). According to $\kappa_{ele} = L\sigma T$, the lattice thermal conductivity (κ_{lat}) can be obtained by subtracting κ_{ele} from the κ_{tot}, and the Lorenz number (L) is set as $1.5\times10^{-8}\,V^2K^{-2}$.[14] The $\kappa_{lat}/\kappa_{tot}$ ratio ranging from 1.0 to 0.73 from 300–730 K indicates that the total thermal conductivity is dominated by the phonon transport. The lattice thermal conductivity slightly decreases with increasing temperature, at 727 K reaching about 0.14 $W m^{-1}K^{-1}$. This is an extraordinarily low value that is even lower than those of all high performance thermoelectrics (for example, 0.5 $W m^{-1}K^{-1}$ in PbTe alloy nanostructured with SrTe and Na[6]). Of course, these κ_{lat} values are measured on polycrystalline samples, which should be lower than the corresponding values on single crystals because the grain boundary effects should decrease the thermal conductivity.

It is interesting that the crystal structure of the title compound is anisotropic, but the TE properties are similar in different directions (the perpendicular/parallel direction of SPS pressure). Materials with anisotropic structures may not always display anisotropic TE properties. For example, when applying low SPS pressure at a relatively low SPS temperature, the anisotropy in the layered Bi_2Te_3 is not really significant.[23]

Density functional theory (DFT) was used to calculate the electronic structure and phonon properties of $CsAg_5Te_3$. The DFT calculated structural parameters of $CsAg_5Te_3$ are $a = b =$ 14.844 Å, and $c = 4.639$ Å, and agree well with the experimental measurements. The DFT calculated direct band gap is 0.53 eV, which is smaller than, but comparable to, the experimental value of 0.67 eV. The band structure reveals several salient features of $CsAg_5Te_3$, such as flattened valence bands and degenerate band extrema at Γ points. The Cs atoms almost make no contribution around E_F and act as electron donors to stabilize the structure (Figure 3).

The band effective mass m^* was obtained from the electronic structure calculations (Figure 3), using the single-band-approximation and the curvature of the conduction band minimum (CBM) or the valence band maximum (VBM). The total density-of-states effective mass is as large

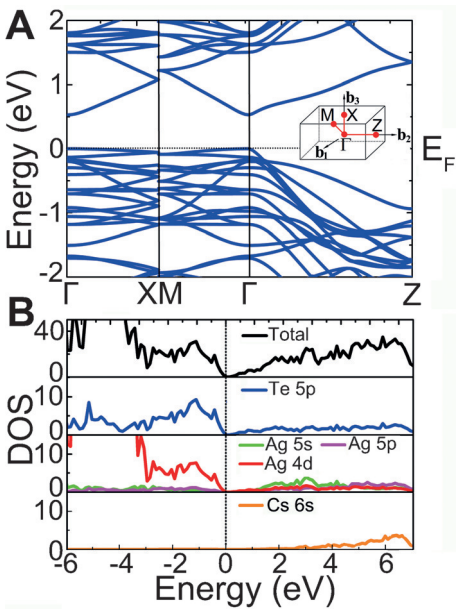

Figure 3. Density functional theory calculations of $CsAg_5Te_3$. A) Calculated electronic band structure of $CsAg_5Te_3$ with the $P4_2/mnm$ space group. Inset: The first Brillouin zone with high-symmetry points (red). Vertical dotted line: E_F; B) Total and partial density of states (DOS, eV/States) of $CsAg_5Te_3$.

as about 1.84 m_0 at the VBM, which when combined with its low hole concentration, yields a very large Seebeck coefficient. The CBM at the Γ-point has a much smaller effective mass of about 0.41 m_0 (Supporting Information, Table S4).

It is interesting to consider the origins of the ultralow lattice thermal conductivity in $CsAg_5Te_3$. It is only around half of the thermal conductivity of so-called phonon-liquid electron-crystal (PLEC) materials α-$Cu_{2-x}S$[13] and β-$Cu_{2-x}Se$.[12] Recently, theoretical studies on the thermal transport of α-Ag_2Te suggested that the thermal conductivity enabled by the Te-Te network interactions is more than 85 % of the total thermal conductivity, whereas that associated with the Ag-Ag network is only a minor contribution.[24] As we will show below, the Te-Te network interactions play a minor role in defining the thermal conductivity of $CsAg_5Te_3$. Instead we find that more important is the behavior of the Ag sublattice and the concerted rattling motions the Ag atoms undergo.

We can estimate the Debye temperature from the ADPs from the following function:[25,26]

$$\frac{\Delta\langle U_{iso}\rangle}{\Delta T} = \frac{3\hbar^2}{\langle m_{at}\rangle k_B \Theta_D{}^2}$$

where U_{iso} is the ADP, $\hbar = h/2\pi$ is the reduced Planck constant, $\langle m_{at}\rangle$ is the average atomic weight, k_B is the Boltzmann constant, Θ_D is the Debye temperature, and T is the absolute temperature The U_{iso} value was determined from the single crystal (Supporting Information, Table S2). The average U_{iso} value of $CsAg_5Te_3$ is calculated to be 0.0306 $Å^2$ for room temperature and 0.0129 $Å^2$ for 100 K, and the average atomic weight mass is 117 amu. These values give a Debye temperature of 118 K for $CsAg_5Te_3$.

The Debye temperature was also estimated from the C_p data, which were measured from 2–300 K (Supporting Information, Figure S5). At low temperatures, the heat capacity C_p can be expressed as:

$$C_p = \alpha T + \beta T^3$$

Here the two terms represent the electron and lattice contributions, respectively. From low temperature, α and β could be obtained by plotting C_p/T as a function of T^2. The intercept value is α and the slope value is β, and, for $CsAg_5Te_3$, these values are 0.01505 $J\,mol^{-1}K^{-2}$ and 0.01254 $J\,mol^{-1}K^{-4}$ respectively (Supporting Information, Figure S5). Then the Debye temperature Θ_D could be calculated through the formula:

$$\Theta_D = \left(\frac{12\pi^4 NR}{5\beta}\right)^{1/3}$$

where N and R denote the number of atoms in the compound formula and the gas constant. The calculated $\Theta_D = 111.7$ K, which is close to the result estimated from ADP.

To quantitatively confirm the above analysis and explore the origin of this low thermal conductivity at the atomic level, we utilize DFT phonon calculations and the Slack model[27] as introduced in the calculations section to more quantitatively evaluate the lattice thermal conductivity of $CsAg_5Te_3$. It is known that the Grüneisen parameters, which characterize the relationship between phonon frequency and crystal volume change, are useful to estimate the lattice anharmonicity and thus helpful to interpret the physical nature of the lattice thermal conductivity behavior.[16,28] Thus the phonon and Grüneisen dispersions were calculated using first-principles DFT phonon calculations within the quasi-harmonic approximation. The $CsAg_5Te_3$ phonon dispersions are calculated using a 144 atom supercell at two volumes, the equilibrium volume V_0 and an isotropically expanded volume 1.015 V_0 (Supporting Information, Figure S6).

The phonon dispersions and Grüneisen dispersions are plotted in Figure 4 A,B. To quantitatively evaluate the anharmonicity, we plot the dispersion of the Grüneisen parameters of acoustic modes in $CsAg_5Te_3$ (Figure 4 B), and find that they are all very large. The average Grüneisen parameter ($\bar{\gamma}$) of each acoustic dispersion are, respectively $\bar{\gamma}_a = \bar{\gamma}_b = 3.9$, $\bar{\gamma}_c = 4.8$ (Supporting Information, Table S5). These values are even larger than the average Grüneisen parameter of SnSe $\bar{\gamma}_a = 4.1$, a compound which has an ultralow lattice thermal conductivity (ca. 0.64 $W\,m^{-1}K^{-1}$ at 300 K).[14] On the basis of the Slack model, the calculated lattice thermal conductivities(K_L) are shown in Figure 4 C. The calculated values of 0.034–0.013 $W\,m^{-1}K^{-1}$ in the temperature range of 300–800 K are close of our experimental values of about 0.2 $W\,m^{-1}K^{-1}$. Besides the rattling model and large Grüneisen parameters, the complex crystal structure of the materials and its large number of atoms (36 per unit cell), also contributes to the low lattice thermal conductivity on the basis of the Slack model.[26]

The ultralow lattice thermal conductivity of $CsAg_5Te_3$ can be attributed to the very strong anharmonicity indicated by the large Grüneisen parameters. Along with the Grüneisen parameters, however, it is insightful to examine the low frequency vibration modes and the specific atoms contributing to them to further understand the physical origin of the ultralow thermal conductivity. The calculated phonon dispersion results show that there are some very low frequency modes at Γ and Z at about 14.6 and 20.2 cm^{-1} that are rattling modes. We call them rattling modes because: 1) there are three rattling signatures of anticrossing points[29,30] between the rattling and longitude acoustic modes along Γ-X, M-Γ, and Γ-Z, as indicated by red arrows in Figure 4 A; and 2) the four Ag3 atoms at the 4 g site vibrate with much larger amplitudes than all other cage atoms of Cs, Te, Ag1, and Ag2. Note that the Ag3 peak has contributions from 4 Ag atoms from the Ag-4*g* site and the Ag2 peak originates from 8 Ag atoms from the 8*i*(a) site. As shown in the Supporting Information, Figure S8 and Table S2, the largest ADP at room temperature for Ag3 is about 62% larger than Cs and 110% larger than Te. The largest ADP of Ag in $CsAg_5Te_3$ is regarded as an evidence of rattling modes, as in the case of La in $La_{0.75}Fe_3CoSb_{12}$.[28] Owing to the much larger bond distances around the Ag3 atoms than Ag1 and Ag2 sites, we see that the Ag3 atoms play a key role in the proposed rattling vibrations. Furthermore, the homogeneity of the sample was assessed by averaging the compositions of 10 different grains of the SPSed sample and taking the average using an EPMA (Supporting Information, Table S6). The result (namely, $Cs_{0.98(2)}Ag_{5.03(3)}Te_3$) is in agreement with the starting composition, to a certain extent, it also shows that Ag3 does not in static disorder. Different from traditional rattling vibration modes, where a lone rattler atom has large oscillations (vibrations) in an oversized cage forming localized Einstein modes,[28] the rattling modes in

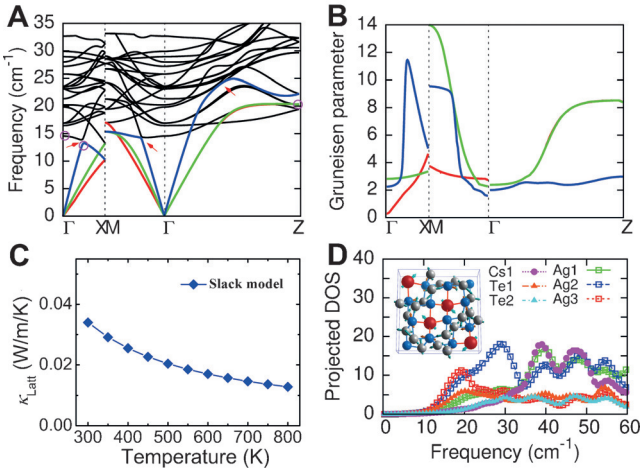

Figure 4. Theoretically calculated phonon and Grüneisen dispersions, and calculated lattice thermal conductivity. A) Phonon dispersion of $CsAg_5Te_3$ at the equilibrium volume V_0. The transverse acoustic phonon scattering branches are labeled in red and green lines and the longitudinal acoustic phonon models are plotted in blue color. The red arrows indicate anticrossing points between rattling modes and LA branches. B) Grüneisen parameters. C) Lattice thermal conductivity. D) Projected phonon density of states of different atomic species. A snapshot of a concerted rattling vibration mode is sketched as an inset in (D). In (A), four circle labels at 14.6 (at Γ), 13.3 (along Γ-X), 20.2 (at Z) and 20.2 (at Z) cm^{-1} show representative concerted rattling modes, which are displayed as movies in Supporting Information.

$CsAg_5Te_3$ involve part or all of the Ag3 sublattice atoms oscillating in phase in a mode we call concerted rattling.

Four representative concerted rattling modes corresponding to four frequencies labeled with circles in Figure 4A are shown as movies in Supporting Information (Figures S9–S12). As can be seen from the movies, for example, for the rattling mode at Γ at 14.6 cm^{-1}, the four Ag3 atoms can be divided into two groups with opposite vibrations of two Ag atoms in each group. Besides the rattling modes at Γ and Z, a mode at the anticrossing point along Γ-X in the LA branch (blue line) also exhibits rattling characteristics, which can be regarded as a mixed mode between a mode at Γ and a mode at X. To quantitatively confirm the strong Ag3 contributions to the low frequency vibrations, we also plotted the projected phonon density of states in Figure 4D. As can be seen the line defined by the red squares the Ag3 atoms indeed exhibit a clear peak around 20 cm^{-1}, which is much higher than the other atoms of Cs, Te, Ag1, and even Ag2. The above analysis suggests the concerted rattling mode from Ag3 site and the strong lattice anharmonicity play a very important role in suppressing the lattice thermal conductivity of $CsAg_5Te_3$.

The special electronic environment of Ag 4*g* atoms induces a very strong anharmonicity, which is expressed as big Grüneisen parameters and also seems to create a rattling mode environment. The rattling modes decrease the phonon group velocity around multiple anticrossing points and reduce the phonon lifetimes due to the Umklapp process, thereby strongly reducing the mean free path.[31,32]

To conclude, $CsAg_5Te_3$ exhibits the lowest lattice thermal conductivity among state-of-the-art thermoelectric materials and reaches a figure of merit of about 1.5 at 727 K, which is among the highest for any single phase bulk material, distinguishing itself as a new promising mid-temperature TE material. $CsAg_5Te_3$, which is a ternary compound, is even more effective in inhibiting heat flow through its crystalline structure than the binary PLEC materials Ag_2Q and Cu_2Q (Q = S, Se, Te) and its low thermal conductivity appears to be different in origin from the so-called Cu/Ag sublattice melting. Instead, a new mechanism producing ultra-low lattice thermal conductivity appears to be operating in $CsAg_5Te_3$ that is associated with the concerted rattling of a group of Ag atoms in the structure. Based on this new insight we anticipate that other materials exist exhibiting similar modes of vibration and exceedingly low thermal conductivities.

Experimental Section

Polycrystalline $CsAg_5Te_3$ samples were prepared by melting the elements Ag (shot, 99.999%, Alfa Aesar), and Te (shot, 99.9999%, Alfa Aesar), and Cs_2Te_3 that was prepared by reacting stoichiometric amounts of the elements in liquid ammonia in a fused silica tube at 1,073 K for 2 h and then cooled to room temperature. Single crystals were obtained. The obtained ingot was ground into fine powders using agate mortar to reduce the grains to less than 4 μm in diameter. The powders were then put inside a 12.7 mm diameter graphite die and densified by spark plasma sintering (SPS, SPS-211LX, Fuji Electronic Industrial Co., Ltd.) at 723 K for 10 min under an axial compressive stress of 50 MPa in vacuum. Highly dense disk-shaped pellets with dimensions of 12.7 mm diameter and ca. 12 mm thickness were obtained. The obtained pellets had relative densities larger than 97% of the theoretical value (7.117 $g\,cm^{-3}$). The powder XRD patterns were taken at room temperature on a Rigaku DMAX 2500 powder X-ray diffractometer by using Cu $K\alpha$ radiation ($\lambda = 1.5418$ Å) and data were analyzed using a profile fitting by a least-squares method employing the computer program GSAS implemented with EXPGUI.[33] Scanning electron microscopy (SEM) images and back-scattering electron (BSE) detector modes using a field emission scanning electron microscope (FE-SEM, JSM6700-F, Japan). The chemical composition of the samples was determined using an electron probe micro-analyzer (EPMA-1600, Japan). Temperature dependent powder XRD patterns were recorded between 300 and 723 K on a Shimadzu XRD-7000. The optical diffuse reflectance spectrum of powdered sample was measured at room temperature using a PerkinElmer Lambda 950 UV/Vis spectrophotometer equipped with an integrating sphere attachment and $BaSO_4$ as a reference. The absorption spectrum was calculated from the reflection spectrum via the Kubelka-Munk function: $\alpha/S = (1-R)^2/2R$, in which α was the absorption coefficient, S was the scattering coefficient, and R was the reflectance.[34] DTA experiments were performed on a computer-controlled Shimadzu DTA-50 thermal analyzer. The electrical resistivity and Seebeck coefficient were measured simultaneously in a low pressure helium atmosphere using a ULVAC-RIKO ZEM-3 instrument system. The thermal diffusivity (D) was measured at 296–773 K by using the laser flash diffusivity method in a commercial Netzsch LFA-457 instrument and the heat capacity (C_p) was obtained using a NETZSCH DTA 404PC. The total thermal conductivity was calculated using the formula $\kappa = D \times C_p \times d$, where d was the sample density, which was determined using the dimensions and mass of the sample and then reconfirmed by measurements using a gas pycnometer (Micromeritics AccuPyc 1340). Low temperature thermal conductivity measurements were carried out over the temperature range of 5–300 K using a longitudinal steady-state technique in a homemade cryostat (for details, see the Supporting Information).The electrical and thermal properties were measured from different parts on the same SPSed pellet with high homogeneity (Figure S2). No significant anistropy was observed parallel or perpendicular to the sintering pressure directions (Figure 1). The Hall coefficient was measured on a K2500-5RSLP Variable Temperature Hall Measurement System under a magnetic field (up to ±1 T) perpendicular to the sample surface.

Acknowledgements

This work was supported by the National Natural Science Foundation of China under Projects (21571020, 20973175, 21233009, 21301175, 21225104, and 91422303) and the NSF of Fujian Province (No. 2015J01071). At Northwestern this work (sample preparation, thermoelectric measurements, DFT calculations) was supported by the Department of Energy, Office of Science Basic Energy Sciences grant DE-SC0014520.

Keywords: concerted rattling · $CsAg_5Te_3$ · thermoelectric materials · tunnel structure · ultralow thermal conductivity

How to cite: *Angew. Chem. Int. Ed.* **2016**, *55*, 11431–11436
Angew. Chem. **2016**, *128*, 11603–11608

[1] T. M. Tritt, *Science* **1999**, *283*, 804.
[2] G. J. Snyder, E. S. Toberer, *Nat. Mater.* **2008**, *7*, 105.

[3] J. P. Heremans, V. Jovovic, E. S. Toberer, A. Saramat, K. Kurosaki, A. Charoenpha kdee, S. Yamanaka, G. J. Snyder, *Science* **2008**, *321*, 554.
[4] J. P. Heremans, B. Wiendlocha, A. M. Chamoire, *Energy Environ. Sci.* **2012**, *5*, 5510.
[5] G. J. Tan, L. D. Zhao, F. Y. Shi, J. W. Doak, S. H. Lo, H. Sun, C. Wolverton, V. P. Dravid, M. G. Kanatzidis, *J. Am. Chem. Soc.* **2014**, *136*, 7006.
[6] K. Biswas, J. Q. He, I. D. Blum, C. I. Wu, T. P. Hogan, D. N. Seidman, V. P. Dravid, M. G. Kanatzidis, *Nature* **2012**, *489*, 414.
[7] G. J. Snyder, M. Christensen, E. Nishibori, T. Caillat, B. B. Iversen, *Nat. Mater.* **2004**, *3*, 458.
[8] K. F. Hsu, S. Loo, F. Guo, W. Chen, J. S. Dyck, C. Uher, T. Hogan, E. K. Polychroniadis, M. G. Kanatzidis, *Science* **2004**, *303*, 818.
[9] J. S. Rhyee, K. H. Lee, S. M. Lee, E. Cho, S. Kim, E. Lee, Y. S. Kwon, J. H. Shim, G. Kotliar, *Nature* **2009**, *459*, 965.
[10] M. K. Jana, K. Pal, U. V. Waghmare, K. Biswas, *Angew. Chem. Int. Ed.* **2016**, DOI: 10.1002/anie.201511737; *Angew. Chem.* **2016**, DOI: 10.1002/ange.201511737.
[11] W. J. Qiu, L. L. Xi, P. Wei, X. Z. Ke, J. H. Yang, W. Q. Zhang, *Proc. Natl. Acad. Sci. USA* **2014**, *111*, 15031.
[12] H. L. Liu, X. Shi, F. F. Xu, L. L. Zhang, W. Q. Zhang, L. D. Chen, Q. Li, C. Uher, T. Day, G. J. Snyder, *Nat. Mater.* **2012**, *11*, 422.
[13] Y. He, T. Day, T. S. Zhang, H. L. Liu, X. Shi, L. D. Chen, G. J. Snyder, *Adv. Mater.* **2014**, *26*, 3974.
[14] S. N. Guin, A. Chatterjee, D. S. Negi, R. Datta, K. Biswas, *Energy Environ. Sci.* **2013**, *6*, 2603.
[15] X. Lu, D. T. Morelli, Y. Xia, F. Zhou, V. Ozolins, H. Chi, X. Y. Zhou, C. Uher, *Adv. Energy Mater.* **2013**, *3*, 342.
[16] L. D. Zhao, S. H. Lo, Y. S. Zhang, H. Sun, G. J. Tan, C. Uher, C. Wolverton, V. P. Dravid, M. G. Kanatzidis, *Nature* **2014**, *508*, 373.
[17] L. D. Zhao, G. J. Tan, S. Q. Hao, J. Q. He, Y. L. Pei, H. Chi, H. Wang, S. K. Gong, H. B. Xu, V. P. Dravid, C. Uher, G. J. Snyder, C. Wolverton, M. G. Kanatzidis, *Science* **2016**, *351*, 141.
[18] J. Li, H. Y. Guo, X. Zhang, M. G. Kanatzidis, *J. Alloys Compd.* **1995**, *218*, 1.
[19] G. Mahan, B. Sales, J. Sharp, *Phys. Today* **1997**, *50*, 42.
[20] K. Kurosaki, A. Kosuga, H. Muta, M. Uno, S. Yamanaka, *Appl. Phys. Lett.* **2005**, *87*, 061919.
[21] S. R. Brown, S. M. Kauzlarich, F. Gascoin, G. J. Snyder, *Chem. Mater.* **2006**, *18*, 1873.
[22] Q. S. Guo, M. C. Chan, B. A. Kuropatwa, H. Kleinke, *Chem. Mater.* **2013**, *25*, 4097.
[23] W. J. Xie, J. He, S. Zhu, T. Holgate, S. Y. Wang, X. F. Tang, Q. J. Zhang, T. M. Tritt, *J. Mater. Res.* **2011**, *26*, 1791.
[24] T. Ouyang, X. Zhang, M. Hu, *Nanotechnology* **2015**, *26*, 025702.
[25] B. C. Sales, B. C. Chakoumakos, D. Mandrus, J. W. Sharp, *J. Solid State Chem.* **1999**, *146*, 528.
[26] B. T. W. Willis, A. W. Pryor, *Thermal Vibrations in Crystallography*, Cambridge University Press, Cambridge, **1975**.
[27] E. J. Skoug, J. D. Cain, D. T. Morelli, *Appl. Phys. Lett.* **2010**, *96*, 181905.
[28] D. T. Morelli, J. P. Heremans, G. A. Slack, *Phys. Rev. B* **2002**, *66*, 195304.
[29] M. Christensen, A. B. Abrahamsen, N. B. Christensen, F. Juranyi, N. H. Andersen, K. Lefmann, J. Andreasson, C. R. H. Bahl, B. B. Iversen, *Nat. Mater.* **2008**, *7*, 811.
[30] J. Dong, O. F. Sankey, C. W. Myles, *Phys. Rev. Lett.* **2001**, *86*, 2361.
[31] T. Tadano, Y. Gohda, S. Tsuneyuki, *Phys. Rev. Lett.* **1996**, *114*, 095501.
[32] C. H. Lee, *J. Phys. Soc. Jpn.* **2006**, *75*, 123602.
[33] "EXPGUI, a graphical user interface for GSAS": B. H. Toby, *J. Appl. Crystallogr.* **2001**, *34*, 210.
[34] G. Kortüm, *Reflectance Spectroscopy*, Springer, Berlin, **1969**.

Received: May 22, 2016
Revised: July 5, 2016
Published online: August 11, 2016

